

LEVEL

fw

Q

AD A 097477

**DEVELOPMENT OF A NOVEL LASER MATERIAL
FOR MINIATURIZED LASER SYSTEMS**

QUARTERLY TECHNICAL REPORT

8 November to 31 December 1980

Sponsored by

DEFENSE ADVANCED RESEARCH PROJECTS AGENCY

DARPA Order No. 4040

Contract No. MDA903-81-C-0034

**DTIC
SELECTED
APR 8 1981**

C

Principal Investigator: Dr. Walter Zwicker (914) 762-0300

Monitored by: Dr. Jefferey L. Paul

Contract Period: 8 Nov. 1980 - 31 Oct. 1982

**APPROVED FOR PUBLIC RELEASE
DISTRIBUTION UNLIMITED**

THE VIEWS AND CONCLUSIONS CONTAINED IN THIS DOCUMENT
ARE THOSE OF THE AUTHORS AND SHOULD NOT BE INTERPRETED
AS NECESSARILY REPRESENTING THE OFFICIAL POLICIES,
EITHER EXPRESSED OR IMPLIED, OF THE DEFENSE ADVANCED
RESEARCH PROJECTS AGENCY OR THE UNITED STATES GOVERNMENT.

Prepared by

PHILIPS LABORATORIES
A Division of North American Philips Corporation
Briarcliff Manor, New York 10510

March 1981

DIE FILE COPY

81 4 8 035

UNCLASSIFIED

SECURITY CLASSIFICATION OF THIS PAGE (When Data Entered)

REPORT DOCUMENTATION PAGE		READ INSTRUCTIONS BEFORE COMPLETING FORM
1. REPORT NUMBER	2. GOVT ACCESSION NO. AD A097477	3. RECIPIENT'S CATALOG NUMBER
4. TITLE (and Subtitle) DEVELOPMENT OF A NOVEL LASER MATERIAL FOR MINIATURIZED LASER SYSTEMS		5. TYPE OF REPORT & PERIOD COVERED Quarterly Technical Report, 8 Nov 1980 to 31 Dec 1980
7. AUTHOR(s) Walter/Zwicker Sel/Colak Jacob/Khurgin		8. CONTRACT OR GRANT NUMBER(s) MDA903-81-C-0034 DARPA Order-4844
9. PERFORMING ORGANIZATION NAME AND ADDRESS PHILIPS LABORATORIES A Division of North American Philips Corp. Briarcliff Manor, New York 10510		10. PROGRAM ELEMENT, PROJECT, TASK AREA & WORK UNIT NUMBERS DARPA Order No. 4040
11. CONTROLLING OFFICE NAME AND ADDRESS Defense Advanced Research Projects Agency 1400 Wilson Boulevard Arlington, Virginia 22209		12. REPORT DATE March 1981
14. MONITORING AGENCY NAME & ADDRESS (if different from Controlling Office) 12 38		13. NUMBER OF PAGES 37
16. DISTRIBUTION STATEMENT (of this Report) APPROVED FOR PUBLIC RELEASE DISTRIBUTION UNLIMITED		15. SECURITY CLASS. (of this report) UNCLASSIFIED
17. DISTRIBUTION STATEMENT (of the abstract entered in Block 20, if different from Report)		15a. DECLASSIFICATION/DOWNGRADING SCHEDULE
18. SUPPLEMENTARY NOTES		
19. KEY WORDS (Continue on reverse side if necessary and identify by block number) Laser material Miniature laser Crystal growth Laser rods Stoichiometric neodymium compounds Laser cavity neodymium		
20. ABSTRACT (Continue on reverse side if necessary and identify by block number) The purpose of this research is to determine which of the various stoichiometric neodymium materials is best suited for the construction of a miniature 1.06 μ m laser. To optimize such a laser, miniature laser rods will be fabricated from single crystals of the most promising materials and evaluated with suitable test circuitry/cavities. For synthesis and crystal growth of the various stoichiometric neodymium compounds, several flux growth furnaces were constructed and two pulling systems permitting "top seeded" crystal		

DTIC
SELECTED
APR 8 1981

387334

YUW

UNCLASSIFIED

SECURITY CLASSIFICATION OF THIS PAGE(When Data Entered)

20. ABSTRACT (Cont'd.)

growth were installed. Preliminary growth experiments on crystals of $\text{NdP}_5\text{O}_{14}$ and $\text{Nd}_{0.9}\text{Y}_{0.1}\text{Al}_3(\text{BO}_3)_4$ were performed, and some of the resulting crystals were evaluated. Equipment was set up for measuring fluorescence lifetimes and emission and absorption spectra and cross-sections. Based on preliminary computer calculations for optimization of the miniature laser cavity, an elliptical cavity and a dual-elliptical cavity were fabricated.

UNCLASSIFIED

SECURITY CLASSIFICATION OF THIS PAGE(When Data Entered)

PREFACE

This work is being performed by Philips Laboratories, a Division of North American Philips Corporation, Briarcliff Manor, New York under the overall supervision of Dr. Rameshwar Bhargava, Director, Exploratory Research Group. Dr. Walter Zwicker, Senior Program Leader for Crystal Growth and Materials Technology, is the Principal Investigator. Mr. Emil Abelaf is responsible for crystal growing; Dr. Sel Colak and Mr. Jacob Khurgin are responsible for materials evaluation as well as laser design and construction.

This program is sponsored by the Defense Advanced Research Projects Agency (DARPA) and was initiated under Contract No. MDA903-81-C-0034. Dr. Jefferey L. Paul is the Contracting Officer's Technical Representative for DARPA.

The work described in this first Quarterly Technical Report covers the period from 8 November to 31 December 1980.

Accession For	
NTIS GRA&I	<input checked="" type="checkbox"/>
DTIC TAB	<input type="checkbox"/>
Unannounced	<input type="checkbox"/>
Justification	
By _____	
Distribution/	
Availability Codes	
Avail and/or	
Special	
A	

SUMMARY

The purpose of this research is to determine which of the various stoichiometric neodymium materials is best suited for the construction of a miniature 1.06 μm laser. To optimize such a laser, miniature laser rods will be fabricated from single crystals of the most promising materials and evaluated with suitable test circuitry/cavities. For synthesis and crystal growth of the various stoichiometric neodymium compounds, several flux growth furnaces were constructed and two pulling systems permitting "top seeded" crystal growth were installed. Preliminary growth experiments on crystals of $\text{NdP}_5\text{O}_{14}$ and $\text{Nd}_x\text{Y}_{1-x}\text{Al}_3(\text{BO}_3)_4$ were performed, and some of the resulting crystals were evaluated. Equipment was set up for measuring fluorescence lifetimes and emission and absorption spectra and cross-sections. Based on preliminary computer calculations for optimization of the miniature laser cavity, an elliptical cavity and a dual-elliptical cavity were fabricated.

TABLE OF CONTENTS

<u>Section</u>	<u>Page</u>
PREFACE.....	3
SUMMARY.....	4
LIST OF ILLUSTRATIONS.....	6
1. INTRODUCTION.....	9
2. MATERIALS PREPARATION AND CRYSTAL GROWTH.....	10
2.1 General Considerations.....	10
2.2 Discussion of Selected Stoichiometric Nd Laser Materials.....	10
2.3 Growth of Crystals of Most Promising Nd Laser Materials.	14
2.3.1 NdP ₅ O ₁₄	14
2.3.2 NdLiP ₄ O ₁₂	15
2.3.3 NdAl ₃ (BO ₃) ₄	15
3. MATERIALS EVALUATION.....	16
3.1 Absorption and Emission Spectra and Cross Section Measurements.....	16
3.2 Fluorescence Lifetime.....	17
4. LASER DESIGN AND CONSTRUCTION.....	19
4.1 Evaluation of Pumping Efficiency.....	19
4.2 Equations Describing Lasing Process.....	21
4.3 Calculation of Energy Stored in Laser Rod.....	24
4.4 Free Generation Mode of Laser Operation.....	26
4.5 Passive Q-Switching Mode of Laser Operation.....	26
4.6 Q-Switching and Frequency-Doubling Mode of Laser Operation.....	26
4.7 Remarks.....	35
5. PLANS FOR NEXT QUARTER.....	36
DISTRIBUTION LIST.....	37

LIST OF ILLUSTRATIONS

<u>Figure</u>	<u>Page</u>
1. Setup for measuring fluorescence spectra.....	16
2. Setup for measuring fluorescence lifetime.....	17
3. Cross-section of a single elliptical cavity.....	20
4. Principal scheme of the $\text{NdP}_{514}\text{O}_{14}$ laser including Q-switching and frequency doubling.....	20
5. Single elliptical cavity efficiency for $2R = 3 \text{ mm}$, $2d = 3 \text{ mm}$ as a function of eccentricity (wall reflectivity is 100%).....	22
6. Single elliptical cavity efficiency for $2R = 3 \text{ mm}$, $2d = 3 \text{ mm}$ as a function of eccentricity (wall reflectivity is 90%).....	22
7. (A) All pumping pulses have a Gaussian shape, an energy of 40 mJ, and different durations. (B) Time evolution of energy stored in the upper laser level.....	25
8. Free generation laser pulses from a laser rod $1 \times 1 \times 10 \text{ mm}$. Output mirror reflectivity is 70% and length of resonator is 10 cm.....	27
9. Free generation laser pulses from a laser rod $1 \times 1 \times 10 \text{ mm}$. Output mirror reflectivity is 50% and length of resonator is 10 cm.....	27
10. Q-switching pulses. Origin of time axis was chosen arbitrarily. Size of rod is $1 \times 1 \times 10 \text{ mm}$ and length of resonator is 10 cm.....	28
11. Phase trajectories for frequency doubled Q-switched laser output. Frequency doubling efficiency is constant, while initial population inversion varies.....	31
12. Phase trajectories for frequency doubled Q-switched laser output. Frequency doubling efficiency is constant, while frequency doubling efficiency varies.....	31
13. Phase trajectories for second harmonic radiation. Frequency doubling efficiency is constant, while initial population inversion varies.....	32
14. Phase trajectories for second harmonic radiation. Initial population inversion is constant, while frequency doubling efficiency varies.....	32

LIST OF ILLUSTRATIONS (Cont'd.)

<u>Figure</u>		<u>Page</u>
15.	Peak second harmonic power vs. initial breakdown for different frequency doubling efficiencies.....	34
16.	Energy of second harmonic radiation vs. initial inversion for different frequency doubling efficiencies.....	34
17.	Pulse duration vs. initial inversion for different frequency doubling efficiencies.....	35

1. INTRODUCTION

The purpose of this work is the development of a novel laser material for miniaturized laser systems. During the first two months, i.e., the present reporting period for this contract, a survey was made which covered the luminescence and chemical properties as well as synthesis and crystal growth processes of all better known stoichiometric neodymium compounds. $\text{NdP}_5\text{O}_{19}$, $\text{NdLiP}_4\text{O}_{12}$, and $\text{NdAl}_3(\text{BO}_3)_4$ were chosen as the most promising candidates. Crystals of these materials will be grown and evaluated for their lasing properties; other materials may also be investigated during the latter part of this contract.

The setup of crystal growth furnaces and equipment for these materials is about 80% complete, and most of the materials and chemicals for their synthesis and growth were received.

Equipment for measuring the optical properties of crystals grown, such as absorption and emission spectra and fluorescence lifetime, was set up and tested.

A computer program was written and tested for studying the influence of cavity parameters, Q-switching, and frequency doubling; expressions for the main output parameters were obtained. The program will be used to predict the main characteristics of miniature lasers and to optimize their parameters.

2. MATERIAL PREPARATION AND CRYSTAL GROWTH

2.1 General Considerations

To be suitable for miniature laser applications, crystals of a stoichiometric rare-earth compound must meet certain basic requirements: the distance of the rare-earth sites in the lattice, lacking a center of inversion, should be at least 5 Å; the gap between valence and conduction bands has to be larger than the energy required to pump the four-level laser cycle of the rare-earth ions; and the other ions of the lattice should not absorb any fluorescence from the rare-earth ions. Table 1 lists the better known stoichiometric Nd compounds which fulfill these requirements, together with their acronyms and some important crystallographic data.

Other properties of the compounds which have to be considered for their practical use in miniature lasers are, e.g., their fluorescence properties such as effective cross section, lifetime, and pump threshold; their stability at ambient; the size of crystals that can be grown; and the cost and ease of growing the crystals. Table 2 lists the fluorescence properties of stoichiometric Nd compounds.

2.2 Discussion of Selected Stoichiometric Nd Laser Materials

$\text{NdP}_{5-14}\text{O}_{14}$ (NdPP) has, besides KNLF, the highest lifetime; most progress in high concentration mini-lasers has been with this material. We have grown, in the past, large crystals of this material and fabricated mini-laser rods from them (Ref. 1). One minor disadvantage of these crystals is their tendency to cleave easily in the (010) plane. Laser rods have to be fabricated, therefore, with a square or rectangular cross section rather than a round one. Although this may not be an ideal shape for a laser rod, output powers of over 80 mJ were obtained from a 2 x 2 x 20 mm laser rod with a 4 J electric input, using a very simple, "nearly confocal" optical cavity (Ref. 2).

Ref. 1. W.R. Zwicker, T. Kovats, R.D. Plahner, W.W. Kruhler and S.R. Chinn, J. Cryst. Growth, 49, 274 (1980).

Ref. 2. S.R. Chinn, "Research Studies on Neodymium Pentaphosphate Miniature Lasers", Final Report prepared for USAERADCOM, Air Force Contract F19628-78-C-0002, 30 Sept. 1978.

Table 1: Comparison of crystallographic data of stoichiometric Nd compounds.

Compound	Acronym	Crystal System	Space Group	Unit Cell	Nd Coord.	Nearest Nd-Nd	
						Distance Å	Nd Conc. (10^{21} cm^{-3})
$\text{NdP}_5\text{O}_{14}$	NPP	monocl.	$P2_1/c$	4	8	5.19	3.96
$\text{NdLiP}_4\text{O}_{12}$	LNP	monocl.	$C2/c$	4	8	5.62	4.37
$\text{NdKP}_4\text{O}_{12}$	KNP	monocl.	$P2_1$	2	8	6.66	4.08
$\text{NdAl}_3(\text{BO}_3)_4$	NAB	trig.	$(R32)$	3	6	5.92	5.43
$\text{NdK}_5(\text{MO}_4)_4$	NKM	trig.	$R\bar{3}m$	1.5	6	5.98	2.32
$\text{NdNa}_5(\text{WO}_4)_4$	NST	tetrag.	$14_1/a$	1.5	8	6.02	2.6
$\text{K}_5\text{NdLi}_2\text{F}_{10}$	KNLF	hexag.	$Pnma$	4	8	6.73	3.6
$\text{Na}_2\text{Nd}_2\text{Pb}_6(\text{PO}_4)_6\text{Cl}_2$	CLAP	orthorhomb.	$P6_3/m$	2	6		3.4

Table 2: Effective cross section σ_E , fluorescence lifetime τ and the lowest observed pump threshold A_T for the $4F_{3/2} \rightarrow 4I_{11/2}$ transition of stoichiometric Nd compounds.

<u>Material</u>	<u>Nd Site Symmetry</u>	σ_E (10^{-19} cm^2)	τ (μs)	A_T (mW)
$\text{NdP}_5\text{O}_{14}$	1	2	135	0,45
$\text{NdLiP}_4\text{O}_{12}$	2	3,2	135	0,20
$\text{NdKP}_4\text{O}_{12}$	1	~ 1,5	100	0,45
$\text{NdAl}_3(\text{BO}_3)_4$	~ 32	10	20	0,55
$\text{NdK}_5(\text{MoO}_4)_4$	($\bar{3}m$), 1	0,7	60	15
$\text{NdNa}_5(\text{WO}_4)_4$	$\bar{4}$	~ 7	85	0,33
$\text{K}_5\text{NdLi}_2\text{F}_{10}$		0,8	300	1,4

$\text{NdLiP}_{4-12}\text{O}_{12}$ (LNP) is very similar to NdPP in its coordination, fluorescence, and lasing properties. It does not have the cleavage problem, however, and fabrication of round laser rods seem feasible. LNP may prove equal or superior to NdPP in device performance, but any advantage may be outweighed by the fact that large crystals are not as easy to grow as those of NdPP.

$\text{NdKP}_{4-12}\text{O}_{12}$ (KNP) is similar to LNP but has a slightly shorter fluorescence lifetime. Another important difference is that KNP has an acentric space group, which in principle allows both linear electro-optic modulation and second-order nonlinear optical effects. Unfortunately, it seems that these effects are too small to permit frequency doubling on a practical scale.

$\text{NdAl}_3(\text{BO}_3)_4$ (NAB) was the first nonphosphate stoichiometric Nd-laser material to be developed. In contrast to the phosphates, the Nd-O coordination is only six-fold, resulting in a substantial deviation from inversion symmetry. The resulting large odd-parity f-d admixture makes the lifetime appreciably shorter. There is, however, a corresponding increase in emission cross section. Like KNP, NAB has an acentric square group. Preliminary measurements performed by us on NAB gave a second-harmonic signal with an intensity of only 0.2 of that of quartz. The signal increased in intensity to twice that of quartz with addition of yttrium to NAB. This can be explained by the fact that pure NAB shows alternating domains consisting of a C2 and C2/c phase, which are both subgroups of C2/m (Ref. 3). Addition of yttrium, however, seems to force NAB to crystallize in a single phase. This fact which is also most important to its lasing properties will be investigated in detail by both x-ray diffraction techniques and measurement of the second harmonic.

$\text{NdK}_5(\text{MoO}_4)_4$ (KNKM) does not exactly belong into this new class of laser materials since there is a statistical 1:1 K^+ , Nd^{3+} occupancy of the rare-earth sites. As a matter of fact, the material would not lase without this statistical distribution. Crystals have a relatively narrow cross section and a high pump threshold. In addition, there are severe

Ref. 3. G. Huber and H.G. Danielmeyer, Proc. Internat. Conf. LASERS '79 p. 619.

thermal problems with this material due to very poor thermal conductivity, and this material is not stable in moist air.

$\text{NdNa}_5(\text{WO}_4)_4$ (NST) may also have a statistical distribution for Nd + Na. However, its large cross section, low threshold, and strong absorption compares favorably with those of the phosphate compound. Unfortunately, the growth of even small optically clear crystals is difficult, and NST offers therefore no advantage over the phosphates.

$\text{K}_5\text{NdLi}_2\text{F}_{10}$ (KNLF) is a recently discovered laser material with a very long fluorescence lifetime. However, its use is limited since the crystals are water soluble and hygroscopic.

$\text{Na}_2\text{Nd}_2\text{Pb}_6(\text{PO}_4)_4\text{Cl}_2$ (CLAP) is a chloroapatite. Apatites form a group of chemical compounds with innumerable members, some of which have been studied for over 15 years as possible laser materials. However, none of them so far has shown to be an outstanding laser host. Many have a low laser damage threshold, and CLAP appears to be, so far, one of the more promising members of this group. Exact fluorescence data has not been published so far for this material but indications are that they compare favorably with those of NdPP. Optically clear crystals, however, again are difficult to grow, and it is questionable whether this compound offers any advantage over the other phosphates.

Summarizing the above, it can be said that NdPP and LNP appear to be the most promising candidates for miniature lasers used in a mini-target designator. Although crystals of NAB are very difficult to grow, their fluorescence properties justify an attempt to produce crystals large enough in size to permit fabrication of laser rods. We have set up equipment, therefore, over the past two months for the growth of crystals of these three compounds which are discussed in the following paragraphs.

2.3 Growth of Crystals of Most Promising Nd Laser Material

2.3.1 $\text{NdP}_5\text{O}_{14}$

$\text{NdP}_5\text{O}_{14}$ does not melt congruently but decomposes before melting at 1400°C. Crystals are grown from a seed in a phosphoric acid flux inside a semi-seal-

ed furnace system. The technique for growing crystals of up to 3 cm in diameter, developed by us previously, has already been described in the literature (Ref. 1). We had established that a very specific temperature profile inside the flux and a precisely controlled evaporation rate of H_2O produced during growth were essential. Five flux-growth furnaces which will fulfill these requirements will be setup; three of these furnaces are already being put into operation. Seeds of appropriate orientation and size have been fabricated.

2.3.2 $NdLiP_4O_{12}$

$NdLiP_4O_{12}$ also melts incongruently, i.e., it disassociates at $970^\circ C$. Crystal-growth techniques used for this material are either flux growth or the Kyropoulos technique (top seeding). Starting materials are Li_2CO_3 , Nd_2O_3 , and $NH_4H_2PO_4$ which decompose during premelting of the mixture to a flux consisting essentially of $LiPO_3$, $Li_4P_2O_7$ and P_2O_5 from which LNP crystallizes during cooling. Composition of the flux can influence, of course, the growth and quality of the crystals. We are presently studying the $P_2O_5 - Li_2O - Nd_2O_3$ phase diagram to optimize flux composition and, thereby, the growth. Since the growth is performed below $950^\circ C$, Kanthal resistance furnaces can be used; we have already set up a three-zone and three one-zone furnace systems for the growth. Since top-seeded growth requires a very slow pull rate, we purchased and set up a crystal puller permitting pulling rates of less than $100 \mu m$ per hour.

2.3.3 $NdAl_3(BO_3)_4$

This compound also decomposes prior to melting, and crystals have to be grown, therefore, from fluxes. Typical fluxes are: $K_2SO_4 - MoO_3 - Nd_2O_3 - Al_2O_3 - B_2O_3$ or $BaO - Nd_2O_3 - Al_2O_3 - B_2O_3$. However, the addition of other foreign and optically inactive ions, e.g., Gd^{3+} , will be necessary in order to obtain a crystallographically single phase of this compound. Since these fluxes have a much higher melting point than the ones used for LNP, we constructed and set up three single and one three-zone platinum furnace systems. Platinum-ware for flux growth of both LNP and NAB has been ordered; parts of this order have already been received.

3. MATERIALS EVALUATION

3.1 Absorption and Emission Spectra and Cross Section Measurements

Absorption. For the absorption measurements, the Beckman ratio-recording spectrophotometer Model DK-24 will be used. This spectrophotometer has interchangeable light sources and photodetectors. The light sources are tungsten-halogen and hydrogen lamps; the photodetectors are photomultipliers for measurements below 700 nm and a lead sulfide cell for above 400 nm. The spectrophotometer allows us to measure the absorption spectra in the 250 - 3000 nm range with a resolution of 3 nm. To obtain precise values of absorption cross-section, 1 mm thick samples of the materials (with nearly parallel sides) will be prepared.

Emission (see Fig. 1). The radiation sources (1) for the emission spectra measurements is either a Bausch & Lomb mercury lamp SP-200 which uses an Osram HB-200 high pressure mercury lamp, or a Bausch & Lomb tungsten-halogen lamp in a standard housing. To obtain nearly monochromatic light, a set of Corning filters (2) and a small Bausch & Lomb monochromator (3) with wide bandwidth (50 nm) is used.

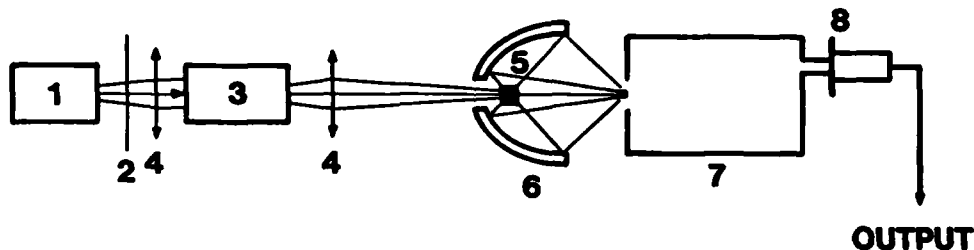


Figure 1. Setup for measuring fluorescence spectra.

The optical system for collimating and focusing of the light beam consists of two quartz lenses (4). The sample (5) is placed into the elliptical mirror at the focal point. This mirror is slightly tilted with respect to the main optical axis of the system in order to decrease the exciting radiation which reaches the entrance slit of the spectrometer placed at the second focal point of the mirror.

The Spex 1701 spectrometer has three different interchangeable gratings which allow us to measure spectra in the 250 nm to 1600 nm range. Near the wavelength of main interest (1.05 μm), the dispersion of the grating is 10 $\text{\AA}/\text{mm}$. The light which passes through the spectrometer is detected by a photomultiplier tube (8) [EMI different types] placed into a housing which can be cooled down to - 40°C. The output of the detector can go directly to an XY recorder or, for weak signals, can be amplified first.

One of the main laser parameters, the cross section of the stimulated emission at 1.05 μm , cannot be determined directly by absorption measurements because of the negligible low population of the lower laser level. We will obtain its value from absorption measurements.

3.2 Fluorescence Lifetime (see Fig. 2)

To excite the Nd^{3+} ions to the upper laser level, an argon-ion laser (1) [Coherent Radiation CR2 supergraphite] is used which is tuned at 5145 \AA , i.e., in one of the absorption bands of Nd^{3+} ions. The radiation of the laser is modulated by an electro-optical modulator (2) [Coherent Associates, Model 3025 with frequency range dc - 25 MHz]. Thus, the sequence of rectangular light pulses with lengths of 10 - 100 μs and repetition rates of 1000 - 100,000 pps can be obtained. The duration and repetition rate of these pulses are appropriate for the lifetime measurements.

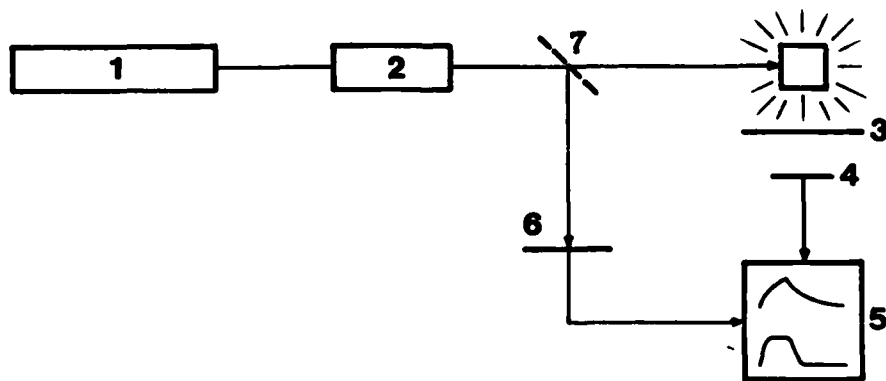


Figure 2. Setup for measuring fluorescence lifetime.

The light beam which passes through the modulator is split into two beams by a beam splitter (7). One of the beams excites the sample, and the other one goes directly to the detector (6) of the reference channel (PIN-10 photodiode U.D.T), connected to the oscilloscope (5).

The light emitted by the sample passes through the Corning filter (3) which has a cutoff wavelength of 8500 Å in order to eliminate the scattered laser radiation from the signal detector (4). The detector (4), which is the same type of PIN photodiode as detector (6), is also connected to the oscilloscope (5).

The fluorescence lifetime in this experiment is determined by the difference between fall times of the two pulses, i.e., the incident pulse and the fluorescence pulse, on the screen of the oscilloscope.

4. LASER DESIGN AND CONSTRUCTION

The main objective of this work is to investigate and optimize the generation of short pulses in the visible and IR ranges, using small Nd-pentaphosphate crystals (laser rods) excited by a flashlamp in an elliptical or double-elliptical cavity (see Fig. 3). The system consists of the laser cavity with crystal, a flashlamp within the cavity, a saturated absorber for the Q-switching, and a crystal for intracavity frequency doubling of the 1.05 μm radiation. The basic structure of the transition levels of the optical materials is shown in Figure 4.

4.1 Evaluation of Pumping Efficiency

To evaluate the pumping efficiency of the system, one has to consider the efficiency of the flashlamp, pump cavity, and laser rod. The total system efficiency is then given by:

$$\eta_p = n_{\text{abs}} \frac{h\nu_p}{P_p} \cdot N_o$$

n_{abs} is the number of pumping-light photons absorbed in 1 cm^3 per 1 second and is given by:

$$n_{\text{abs}} = \frac{1}{V} \int dv \int \frac{P_c}{S} \eta_{\text{fl}}(\nu) (h\nu)^{-1} \eta_c \alpha(\nu) \exp(-r\alpha(\nu)) dV \quad (1)$$

P_p = power consumed by flashlamp.

N_o = density of Nd^{3+} ions

$\frac{h\nu_p}{P_p}$ = average frequency of pump radiation exciting

$$\text{the laser rod} = \int \nu \eta_{\text{fl}}(\nu) \alpha(\nu) d\nu$$

Therefore, the total system efficiency becomes,

$$\eta_p = \eta_c \cdot V^{-1} \iint \eta_{\text{fl}}(\nu) \nu^{-1} \alpha(\nu) \exp(-r\alpha(\nu)) d\nu dV \cdot (SN_o)^{-1} \int \nu \eta_{\text{fl}}(\nu) \alpha(\nu) d\nu \quad (2)$$

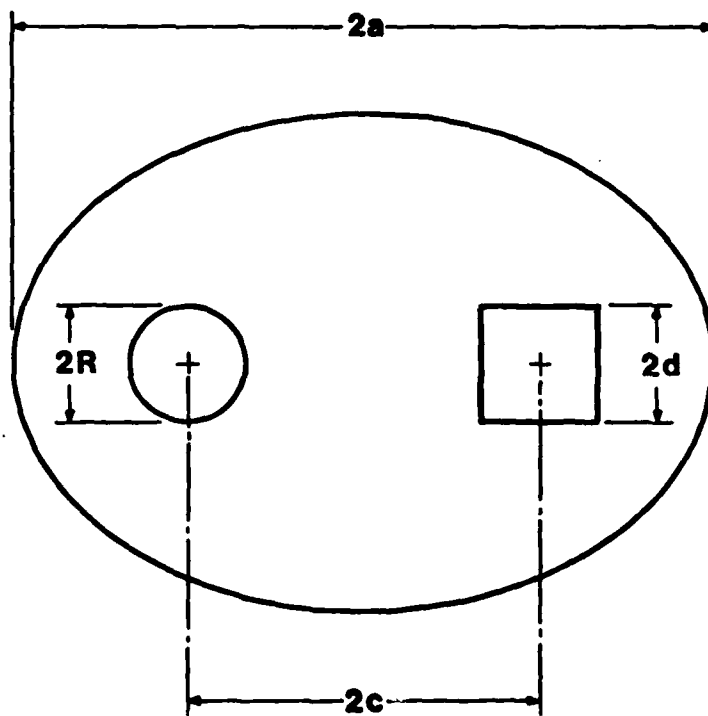


Figure 3. Cross-section of a single elliptical cavity.

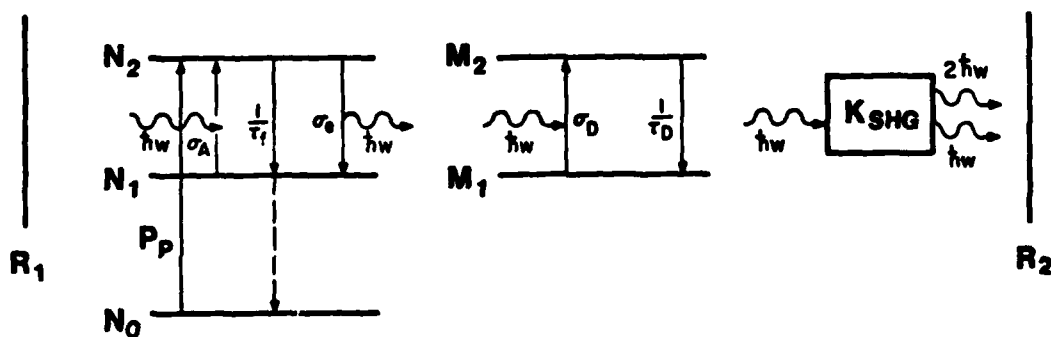


Figure 4. Principal scheme of the NdP₅O₁₄ laser including Q-switching and frequency doubling.

where

- V = rod volume
- $\eta_{fl}(\nu)$ = spectral emission of flashlamp per unit of applied power
- $\alpha(\nu)$ = absorption coefficient
- S = rod surface area
- r = distance from crystal surface
- η_c = geometrical efficiency of cavity

The value for the η_c was determined for an elliptical cavity (see Fig. 3) with the following parameters:

- C = distance between foci
- e = excentricity
- 2R = lamp diameter
- 2d = size of rod

The calculation of the pump cavity geometrical efficiency was performed by the method of random beams. It takes into account the losses on cavity walls together with the reflection and refraction of the crystal surface. The results are shown in Figures 5 and 6. Using these results and taking into account the dimensions of the flashlamp and the laser rod, we designed two cavities with optimal dimensions. One of the cavities is a single-elliptical cylinder; the other is a double-elliptical cylinder.

4.2 Equations Describing Lasing Process

The equations describing the energy transfer between the laser rod, the saturated absorber, and the intracavity frequency doubler are:

$$\frac{dN_2}{dt} = -c\sigma_e \rho N_2 + c\sigma_a \rho N_1 - \frac{N_2}{\tau_F} + N_0 P_p \eta_p / h\nu_p \quad (3.1)$$

$$\frac{d\rho}{dt} = \frac{l}{L} c\sigma_e \rho N_2 - \frac{l}{L} c\sigma_a \rho N_1 - \frac{\rho}{\tau_Q} - c\sigma_o (M_1 - M_2) \frac{l}{L} \rho + \rho_{sp} - \frac{c}{2L} \alpha \rho^2 \quad (3.2)$$

$$\frac{dM_1}{dt} = -c\rho\sigma_o M_1 + \frac{M_2}{\tau_D} \quad (3.3)$$

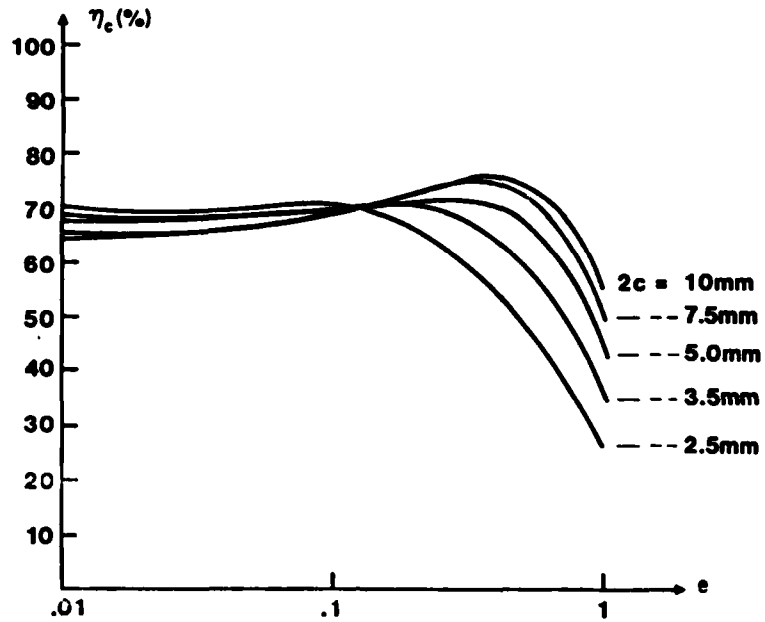


Figure 5. Single elliptical cavity efficiency for $2R = 3$ mm, $2d = 2$ mm as a function of eccentricity. (Walls reflectivity is 100%.)

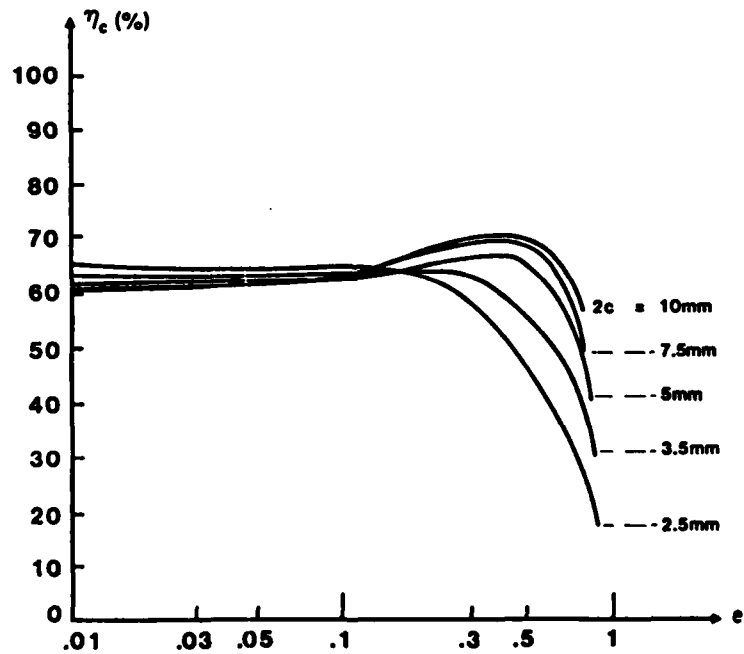


Figure 6. Single elliptical cavity efficiency for $2R = 3$ mm, $2d = 2$ mm as a function of eccentricity. (Walls reflectivity is 90%.)

$$M_1 + M_2 = M_0 \quad (3.4)$$

$$N_1 + N_2 + N_0 = N \quad (3.5)$$

- where:
- N_0 = population density of ground state
 - N_1 = population density of lower laser level
 - N_2 = population density of upper laser level
 - N = total population of Nd^{3+} ions
 - M_1 = population density of lower level of dye
 - M_2 = population density of upper level of dye
 - M_0 = population density of dye molecules
 - l = length of laser rod
 - l_0 = length of dye cell
 - σ_e = cross section of emission on laser wavelength
 - σ_a = cross section of absorption process on laser wavelength
 - σ_D = cross section of absorption from lower dye level (singlet)
 - ρ = photon density in resonator
 - τ_f = fluorescence lifetime of upper laser level
 - τ_Q = photon lifetime in resonator
 - = $2L/(C(L' - \ln R))$, where
 - L = resonator length,
 - L' = cavity losses
 - R = reflectivity of output mirror
 - τ_D = fluorescence lifetime of upper dye level (Q-switch response time)
 - P_p = pumping consumed by flashlamp
 - ρ_{sp} = spontaneous emission contribution

$$\rho_{sp} = \frac{\chi \cdot N_2}{\tau_{sp}}$$

where:

- τ_{sp} = spontaneous decay time $\tau_{sp} > \tau_f$
- $\chi = A_m/(\pi L^2)$, where A_m = size of mode spot on output mirror.
- α = frequency doubling efficiency of SHG crystal in laser resonator.

These processes are modeled according to the energy level diagram given in Figure 4. These expressions will be used to obtain an optimized design for the laser oscillation.

4.3 Calculation of Energy Stored in Laser Rod

To be able to calculate the maximum output energy obtainable from the laser rod, we first take the power absorbed by the rod as given in Figure 7a. This power is calculated by assuming that the flashlamp input energy is, $\int P_p dt = 1 \text{ J}$, and that the pumping light distribution inside the rod is homogeneous. The dimensions of the rod are 1 mm x 1 mm x 10 mm. The total power absorbed by the rod is:

$$P_{\text{abs}} = N_o V \eta_p \times P_p, \quad (4)$$

and the following assumption has been made according to the experimental data and calculations of Section 4.1.

$$N_o V \eta_p = 0.04$$

It is also assumed that the flashlamp light output has a Gaussian shape in time with different durations as given in Figure 7a. Each pulse contains the same total energy, viz., 40 mJ.

To obtain the value of stored energy without radiation one has to solve Eq. (3) without the first two terms. The value of the stored energy is:

$$E_s t = V \cdot h\nu \cdot \Delta N_{\text{eff}} \quad (5)$$

where, $\Delta N_{\text{eff}} = N_2 - \frac{\sigma_a}{\sigma_e} N_o \exp(-E_1/kT)$,
 E_1 = energy of lower laser level.

In Figure 7b the energy stored on the upper laser level versus the time for different pumping pulse durations is given. It is seen that the higher energies can be achieved by shortening the flashlamp pulse. Nevertheless, even with such a long pulse duration as 100 μs , the high gain (up to 1.3 cm^{-1}) can be achieved. Because of the large cross-section emission, this high gain corresponds to relatively small stored energy between 10 and 15 mJ.

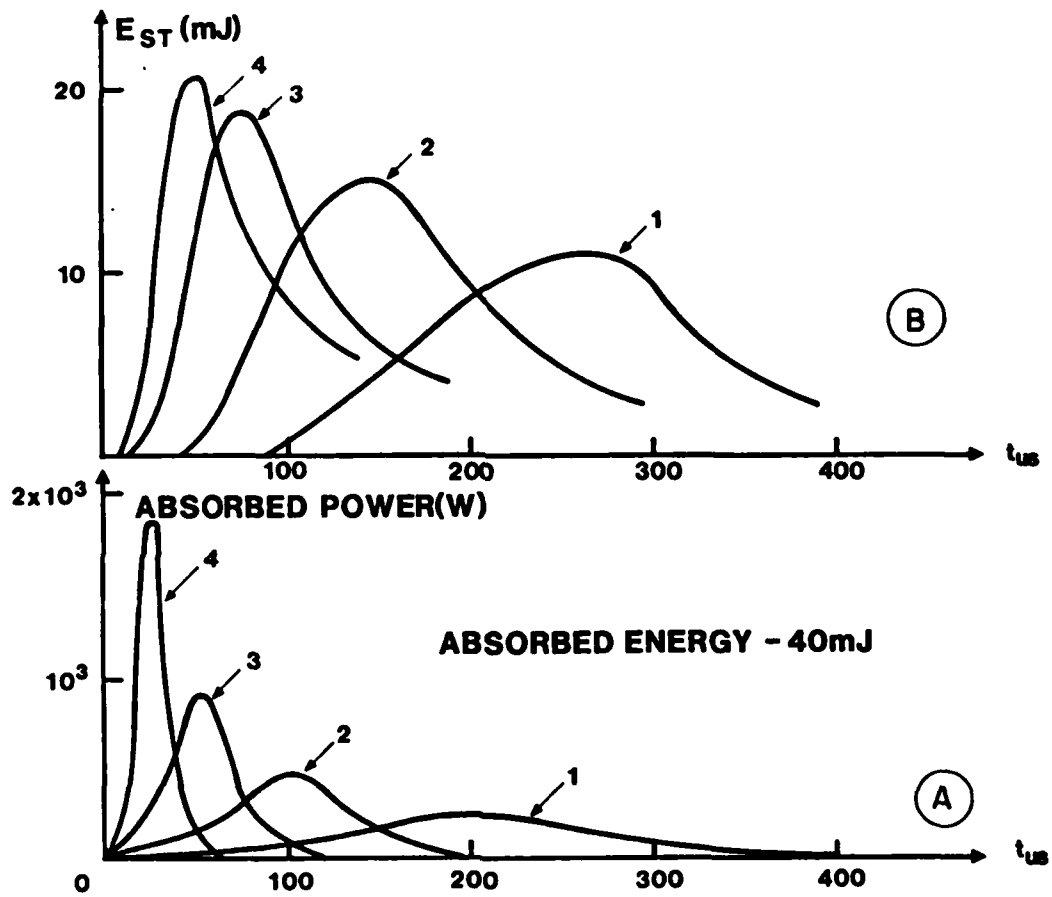


Figure 7. (A) All pumping pulses have a Gaussian shape, an energy of 40 mJ, and different durations. (B) Time evolution of energy stored in upper laser level.

4.4 Free Generation Mode of Laser Operation

The behavior of the laser system in the regime of free generation has been studied. The results of the calculations are shown in Figures 8 and 9. These results give us the opportunity to choose the optimal output mirror reflectivity. It is seen that while there is a possibility of obtaining good output energy, the output power is relatively small and we cannot eliminate oscillation of the output pulse.

4.5 Passive Q-Switching Mode of Laser Operation

The passive Q-switching with a dye cell has also been studied using the set of Equations (3); the result is shown in Figure 10. A high-power sharp pulse can be obtained, and the optimum reflectivity of the output mirror can also be determined.

From the results of Section 4.3, the optimum value for parameter $l_{D^0}^M$ under no oscillation condition,

$$(l_{D^0}^M)^{\text{opt}} = \frac{L}{c\sigma_D} \left\{ \frac{l}{L} c\Delta N_{\text{eff}}^m \sigma_e - \frac{1}{\tau_Q} \right\} \quad (6)$$

where, ΔN_{eff}^m = maximum value of the effective population inversion achieved during pumping pulse. If $l_{D^0}^M = (l_{D^0}^M)^{\text{opt}}$, we obtain an output pulse of minimum length and maximum power. If this value is significantly more than optimum value, the lasing threshold cannot be achieved. If the value of $l_{D^0}^M$ is significantly less than optimum value, we will have two or more smaller pulses, and upon further decreasing $l_{D^0}^M$ we will obtain the free lasing.

4.6 Q-Switching and Frequency-Doubling Mode of Laser Operation

The very short pulse which can be obtained using the Q-switching has a number of disadvantages, especially when it is to be detected. To make the pulse longer while keeping the high energy, we should use some intercavity nonlinear process. The nonlinear losses should increase when the photon density in the resonator increases, thereby decreasing the speed of the upper-laser-level decay. Among the other processes, the intracavity

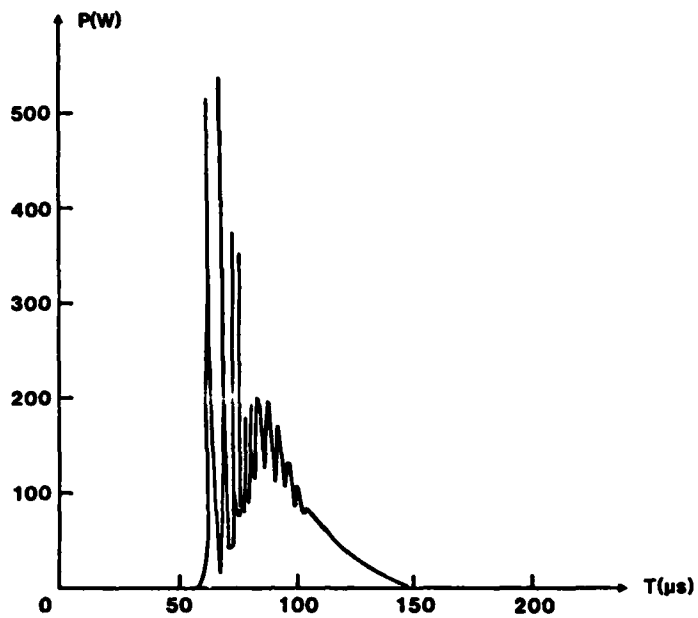


Figure 8. Free generation laser pulse from a laser rod 1 x 1 x 10 mm. Output mirror reflectivity is 70% and length of resonator is 10 cm.

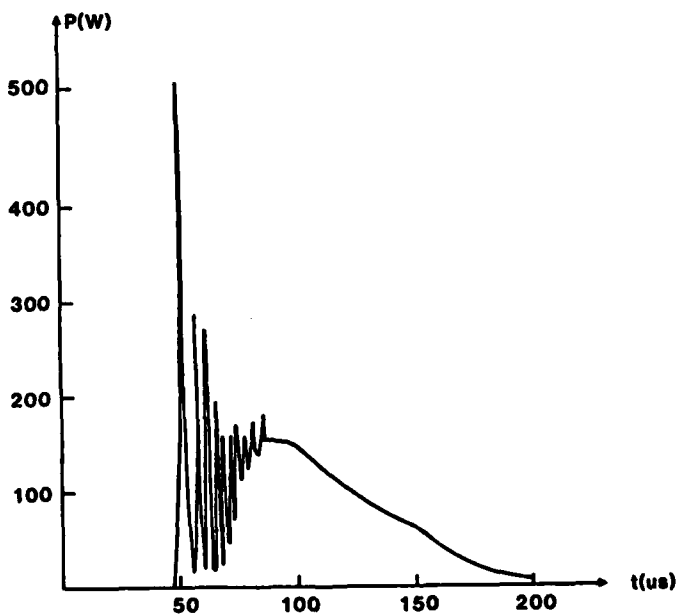


Figure 9. Free generation laser pulse from a laser rod 1 x 1 x 10 mm. Output mirror reflectivity is 50% and length of resonator is 10 cm.

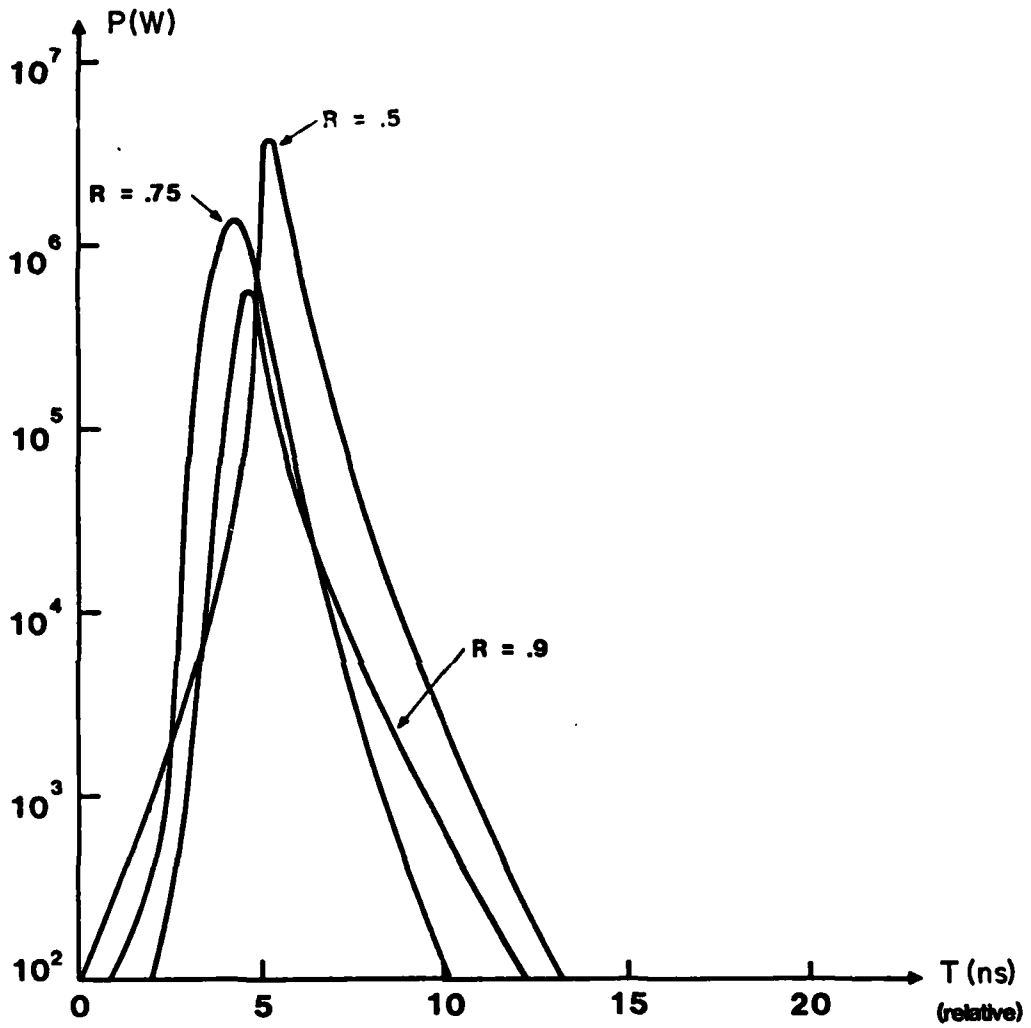


Figure 10. Q-switching pulses. Origin of time axis was chosen arbitrarily. Size of rod is 1 x 1 x 10 mm and length of resonator is 10 cm.

frequency doubling has obvious advantages. The most important one is that its nonlinearity does not mean the loss of energy, but rather the output coupling of the laser. We studied this process both analytically and on a computer. It is assumed that:

- A certain value of initial population inversion ΔN^0 has been reached before generation started. This value can be determined using the calculations of Section 4.3
- The value of the dye cell parameters, $l M_0$, is chosen to be optimal (see Sect. 4.5) and τ_D the dye response time is small. This means that when ΔN_{eff} reaches the initial value ΔN^0 , the dye cell is saturated instantaneously.

Under these conditions, the set of equations (3) can be written as:

$$\frac{dn}{d\tau} = -\rho'n \quad (7.1)$$

$$\frac{d\rho'}{d\tau} = \rho'n - \rho' - K\rho'^2 \quad (7.2)$$

where: $n = \Delta N_{eff} / \Delta N_{TR}$

$\Delta N_{TR} = \frac{L}{l} c\sigma_e \tau_Q$ threshold population inversion density

$$\rho' = \frac{\rho}{\rho_{SAT}} = \frac{I_{FUND}}{I_{SAT}}$$

$\rho_{SAT} = (c\sigma_e \tau_Q)^{-1}$ saturating photon density in the cavity

I_{FUND} = power density of first harmonic radiation in the cavity,
 $I_{FUND} = ch\nu\rho$

I_{SAT} = saturating value of power density of first harmonic radiation
in cavity, $I_{SAT} = ch\nu\rho_{SAT}$

$$\tau = t/\tau_Q$$

$K = K_{SHG}$ normalized coefficient of the SHG efficiency

$$K = \frac{\alpha}{2\sigma_e L} \quad (8)$$

To eliminate time as a parameter, we divide Eq. (7.1) by (7.2) and obtain,

$$\frac{d\rho'}{dn} = \frac{1}{n} + K \frac{\rho'}{n} \quad (9)$$

The solution of Eq. (9) is:

$$\rho' = \frac{K(n_0 - 1) + 1}{K(1 - K)} \left\{ \left(\frac{n}{n_0} \right)^k - \frac{(n - 1)K + 1}{(n_0 - 1)K + 1} \right\} \quad (9a)$$

if $K = 0$

$$\rho' = \ln \left(\frac{n}{n_0} \right) - (n - n_0) \quad (9b)$$

if $K = 1$

$$\rho' = \left[\frac{n}{n_0} - n \ln \left(\frac{n}{n_0} \right) - 1 \right] \quad (9c)$$

where:

$$n_0 = \frac{\Delta N^0}{\Delta N_{TR}}$$

These solutions are shown in the phase diagrams of Figures 11 - 14, where every point represents one state of the system. We can see that the larger the K , the less the fundamental frequency power inside the cavity, but the second harmonic power which (in normalized form) is given by,

$$\rho'_{SHG} = \frac{1}{2} K \rho'^2 = \frac{1}{L'} \cdot \frac{I_{SH}}{I_{SAT}} \quad (10)$$

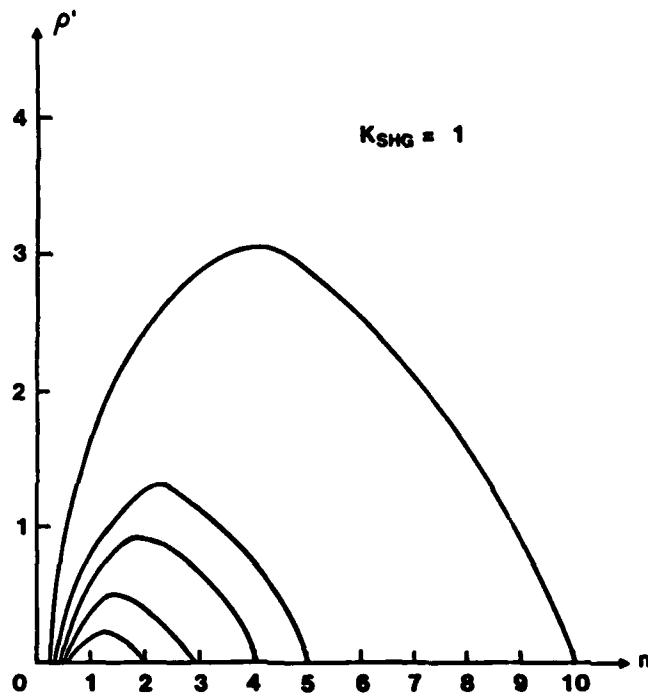


Figure 11. Phase trajectories for frequency doubled Q-switched laser output. Frequency doubling efficiency is constant, while initial population inversion varies.

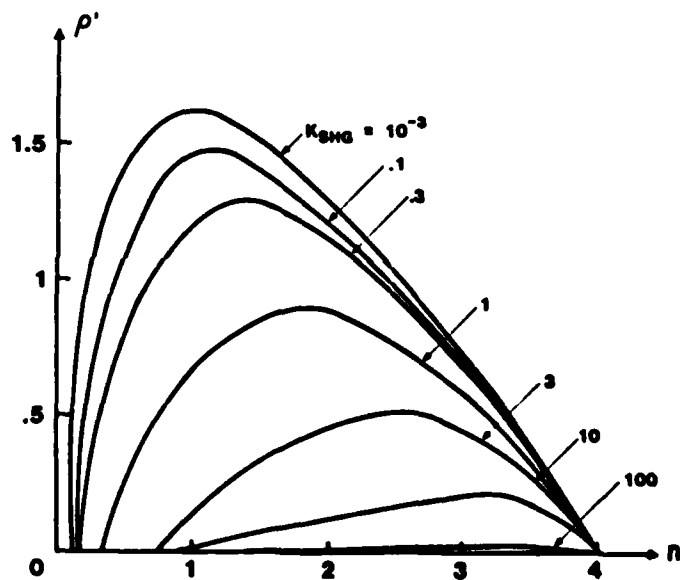


Figure 12. Phase trajectories for frequency doubled Q-switched laser output. Frequency doubling efficiency is constant, while frequency doubling efficiency varies.

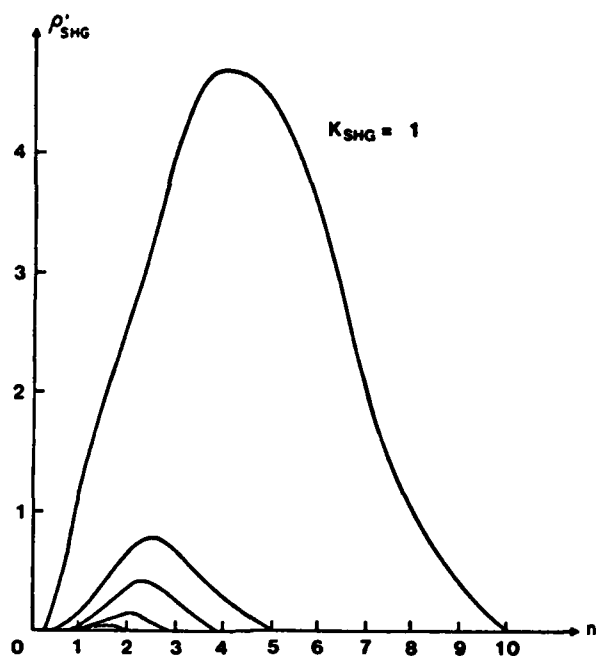


Figure 13. Phase trajectories for second harmonic radiation. Frequency doubling efficiency is constant, while initial population inversion varies.

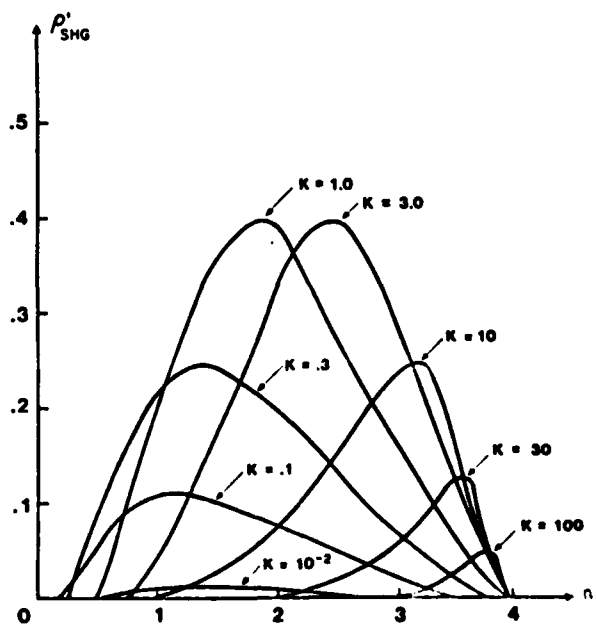


Figure 14. Phase trajectories for second harmonic radiation. Initial population inversion is constant, while frequency doubling efficiency varies.

has a maximum which depends on the initial inversion.

In Figures 15, 16 and 17, one can see the variations of the peak power, pulse energy, and pulse duration. The normalized peak power density is:

$$\rho'_{SHMAX} = \frac{1}{L'} \frac{I_{SH}^{MAX}}{I_{SAT}} \quad (11)$$

The normalized energy density is:

$$E'_{SH} = \frac{1}{L'} \cdot \frac{E_{SH}}{I_{SAT} \tau_Q} = \frac{1}{2} \int \rho'_{SH} \cdot d\tau \quad (12)$$

The normalized time is:

$$\tau = \frac{t}{\tau_Q} \quad (13)$$

Increasing K over 1 does not change the pulse energy significantly, but it can make the pulse much longer.

The maximum energy that can be extracted from the medium with initial population inversion ΔN_0 and with a cavity that has certain threshold inversion N_{TR} is:

$$E_{SHMAX} = h\nu (\Delta N_0 - \Delta N_{TR} - \Delta N_{TR} \ln \left(\frac{\Delta N_0}{N_{TR}} \right)) V_m \quad (14)$$

where V_m = volume of the laser mode in the rod. Thus, for example, if we have a cavity with a threshold value of $0.5 \times 10^{19} \text{ cm}^3$ and a pumping system with an initial inversion up to $2.0 \times 10^{19} \text{ cm}^3$, then the second-harmonic energy for a laser rod with dimensions 1 mm x 1 mm x 10 mm is in the order of 10 mJ.

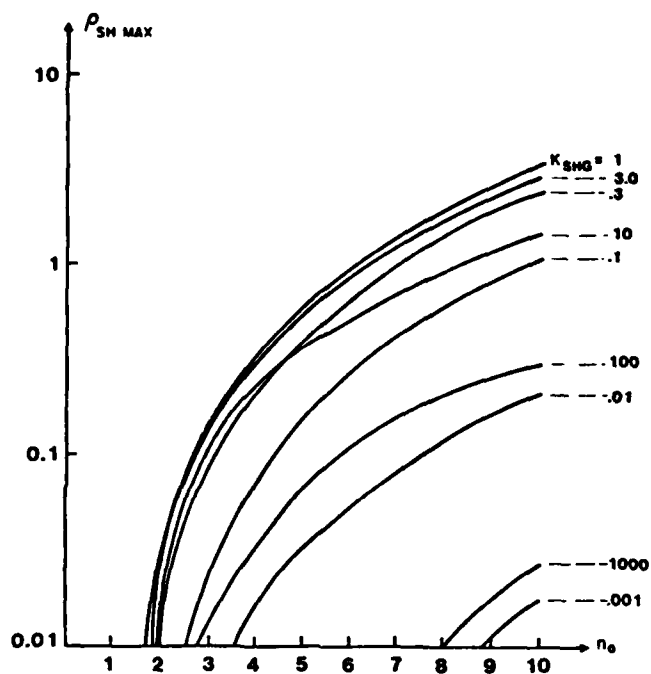


Figure 15. Peak second harmonic power vs. initial breakdown for different frequency doubling efficiencies.

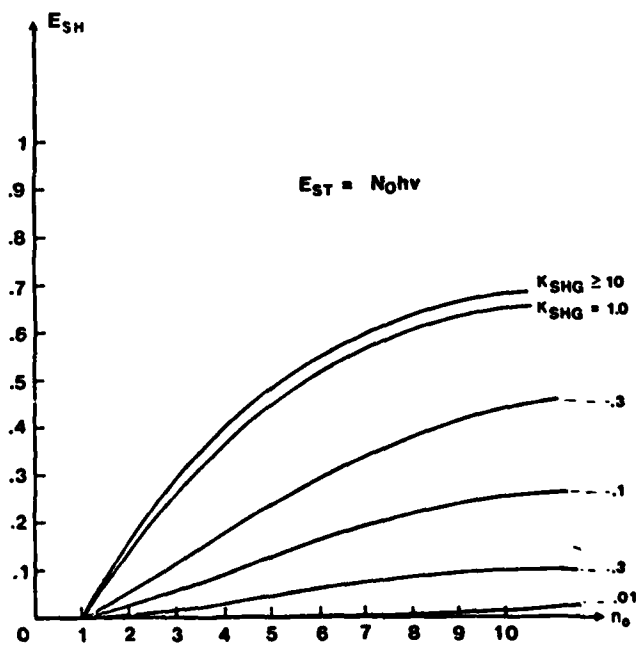


Figure 16. Energy of second harmonic radiation pulse vs. initial inversion for different frequency doubling efficiencies.

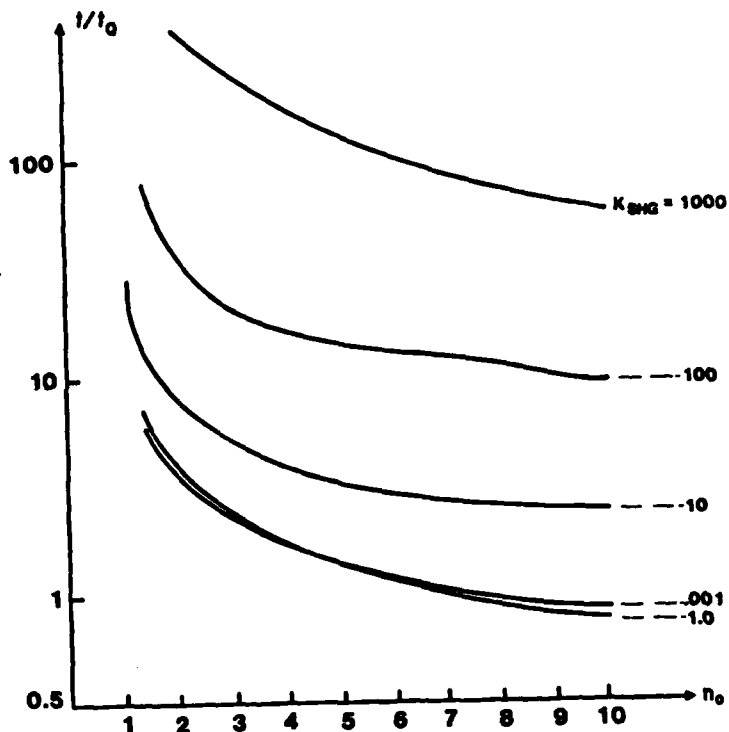


Figure 17. Pulse duration vs. initial inversion for different frequency doubling efficiencies.

4.7 Remarks

The computer program for evaluating the energy parameters of the neodymium pentaphosphate laser was written and tested. With this program, the influence of the cavity parameters and Q-switching as well as frequency-doubling processes, has been studied, and expressions for the main output parameters were obtained. The results of this study will help us to predict the main characteristics of the laser and to optimize some of the parameters.

5. PLANS FOR NEXT QUARTER

- a. Complete construction of crystal growth furnaces and associated equipment.
- b. Start growth of NdPP crystals large enough for fabrication of laser rods (2 x 2 x 15 mm and 2 x 2 x 20 mm).
- c. Start growth of LNP crystals large enough to be seeds for top-seeding experiments.
- d. Evaluate fluorescence properties of crystals produced.
- e. Construct and assemble components for a brassboard-mounted miniature laser.

DISTRIBUTION LIST

	<u>Copies</u>
Director Defense Advanced Research Projects Agency Attention: TIO/Admin. 1400 Wilson Blvd. Arlington, Virginia 22314	(3)
Dr. Jefferey L. Paul DELNV-L Night Vision & Electro-Optics Laboratories Fort Belvoir, Virginia 22060	(1)
Defense Documentation Center Cameron Station Alexandria, Virginia 22314	(12)
TACTEC Battelle Memorial Institute 505 King Avenue Columbus, Ohio 43201	(1)